Available online at www.sciencedirect.com
ScienceDirect
Sensors and Actuators B 128 (2008) 613–621
SENSORS AND ACTUATORS B CHEMICAL
www.elsevier.com/locate/snb

Passive flow switching valves on a centrifugal microfluidic platform

Jitae Kim, Horacio Kido, Roger H. Rangel, Marc J. Madou *

Department of Mechanical and Aerospace Engineering, University of California, Irvine, CA 92697, USA

Received 31 July 2006; received in revised form 14 June 2007; accepted 12 July 2007
Available online 25 July 2007

Abstract

In this paper we present two different methods for a passive flow switching valve on a centrifugal microfluidic platform, which controls the direction of a flowing liquid at a junction where a common inlet and two outlet channels meet. Switching of the flow can be performed either by relying on the Coriolis force that changes its pointing direction, perpendicular to the flow direction, with the rotational direction of a disk in a double layered arrangement at a symmetrical junction, or by means of the fluidic capacitance of an air pocket trapped between two fluids at a non-symmetric junction. This flow-switching valve, when combined with affinity-based separation techniques (e.g., adsorption of DNA on a silica matrix, followed by elution), has great potential in rapid bioassays and biomedical diagnostic applications that require the extraction of specific target biomoleclues.

Keywords: Flow switching valve; Microfluidics; Centrifugal; Coriolis; Air pocket

1. Introduction

There is a wide interest in micron-scale integrated chemical/biochemical analysis or synthesis systems, also referred to as lab-on-a-chip [1] systems. Essential tasks required in these devices are sample transport [2–4] and separation [5,6] as liquids need to move through fluidic paths for reaction (i.e., mixing of sample and reagent) and detection. Those tasks are carried out through carefully controlled pumping and valving events. Extensive efforts have been made to develop simple and reliable micro pumping/valving schemes [7–9] that can be employed in microfluidic systems for chemical and biological analysis. Most integrated microfluidic systems rely on valves that are capable of accurately controlling fluid flows within the fluidic networks. In general, microvalves are categorized into two types: active valves [10–12] and passive valves [13,14]. Active valves are often robust and reliable but typically require moving parts and external actuation mechanisms that make the system inherently more complex and difficult to integrate. Alternatively, passive valves are simpler in operation and more convenient to use in integrated systems in that the operating principle of those valves is based on liquid–surface interactions (i.e., hydrophobic and hydrophilic) and specific geometric designs. This type of valves has been widely used for controlling the release and flow of liquids on a centrifugal fluidic platform [15,16]. A large number of the microvalves that have been developed, however, only feature a stop/release function while there has been an increasing demand for more sophisticated and versatile microfluidic functions to perform more complicated tasks.

In this paper, we introduce a centrifuge-based microfluidic valve that controls the direction of liquid flow at a junction comprising a common inlet and two outlet channels. The switching valve is intended not only to keep a liquid in a reservoir on a microfluidic disk at rest but also to move it only into a selected chamber during rotation of the disk. Here, we present two different methods of flow valving: Coriolis force in a double-layered structure having wider and thicker outlet chambers (Fig. 1) and fluidic capacitance of an enclosed gas pocket in a channel structure in which two outlet channels are non-symmetric and have different entrance widths (Fig. 5).

These centrifuge-based switching valves have great potential in the fields of clinical diagnostics and biological analysis where specific biomoleclues must be separated from a complex mixture.

* Corresponding author. Tel.: +1 949 824 6585; fax: +1 949 824 8585.
E-mail address: mmadou@uci.edu (M.J. Madou).

0925-4005/$ – see front matter © 2007 Published by Elsevier B.V.
doi:10.1016/j.snb.2007.07.079

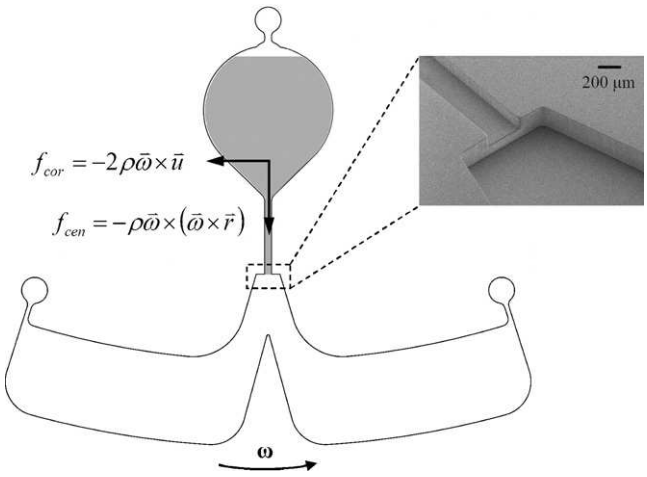

Fig. 1. Illustrative view of two types of forces (centrifugal and Coriolis) acting on a liquid flowing through a microchannel on a rotating disk and a SEM image of a double-layered junction coupled at one end to an inlet channel (and a reservoir) and coupled at another end to two symmetric outlet chambers.

2. Materials and methods

2.1. Fabrication

Polydimethylsiloxane (PDMS) has attracted enormous interest for prototyping of microfluidic devices as various structures such as microchambers and microchannels can be easily molded using PDMS replicating techniques [17]. SU-8, a negative tone photoresist, has been widely used as a master mold for the PDMS replication due to its excellent ultraviolet (UV) transparency facilitating the fabrication of high aspect ratio structures [18] using standard UV lithography.

In our current application, an SU-8 mold having double layer was fabricated using SU-8 100 (Microchem Inc.) on a 6 in. Si wafer (Addison Engineering, CA). The first layer (160 μm thick) comprising reservoirs, inlet channels, and alignment marks, was processed up to the UV exposure step immediately followed by spin-coating of the second layer (270 μm thick). This procedure was adapted after our observation that spin-coating of SU-8 resist for the second layer over the first layer that was already developed, causes severe topology problems such as non-uniform thickness and uncovered regions around the existing structures. Note that the prebake step of the second layer substitutes for the post exposure bake of the first layer. Since cross-linked SU-8 has a lower optical transparency than the unexposed surroundings, the alignment marks buried in the unexposed second layer of SU-8 can be readily observed. The two layers were then exposed to UV light to form outlet chambers (430 μm thick) and were developed after the post exposure bake.

The PDMS precursor and curing agent (Dow Corning) were mixed thoroughly in a weight ratio of 10:1. After degassing the mixture in vacuum, it was poured and cured on the SU-8 master mold with a rim fashioned around the substrate to contain the liquid PDMS. A microfluidic disk was completed by sandwiching the micromachined PDMS sheet between two polycarbonate disks with an adhesive film.

2.2. Flow valving: Coriolis force

Until recently [19–21], the Coriolis force has not been extensively explored for microfluidic functions, as opposed to the centrifugal force which has been dominantly cited as a fluid propulsion mechanism in a centrifuge platform. In fact, a rotating microfluidic disk generates two types of inertial forces acting on the moving liquid in its fluidic path: a centrifugal force in a radially outward direction and a Coriolis force perpendicular to flow direction as shown in Fig. 1. The transversal Coriolis force is exploited to switch the flow direction of the liquid in what we call "passive flow switching valve", by changing the rotational direction of the disk. Fig. 1 also shows a double layer arrangement of a junction coupled at one end to a common inlet channel and at the other end to two outlet chambers. In this section, we present a 3-dimensional analysis of the flow rate of liquid (2-dimensional analysis was performed in the previous works [19–21], i.e., by taking an infinity for the channel depth) arriving at the junction and experimentally find a minimum angular frequency at which the flow valving is always ensured.

2.2.1. Navier–Stokes equations in a rotating frame of reference

For a rotating system, it is often convenient to observe the system from a center of the rotation (i.e., an origin of the rectangular coordinates revolving on an axis of the rotation). The result of being in such a non-inertial frame is the appearance of two fictitious forces—centrifugal and Coriolis forces.

The position and velocity vectors in a rectangular coordinate system are defined as:

$$\vec{r} = z\langle\vec{k}\rangle + x\langle\vec{i}\rangle + y\langle\vec{j}\rangle \tag{1}$$

$$\vec{u} = u\langle\vec{k}\rangle + v\langle\vec{i}\rangle + w\langle\vec{j}\rangle \tag{2}$$

where $\vec{k}$, $\vec{i}$, and $\vec{j}$ are the unit vectors with each parallel to channel length, width, and depth, respectively, and have their origins at a point where the axis of the rotation and the center of the channel cross-section meet (see Fig. 2). Suppose our disk is rotating at a constant angular velocity of $\vec{\omega}$. Then, accelerations measured from the two different frames are related by:

$$\vec{a}_F = \vec{a}_R + \vec{\omega}\times(\vec{\omega}\times\vec{r}) + 2\vec{\omega}\times\vec{u}_R \tag{3}$$

where $\vec{\omega}\times(\vec{\omega}\times\vec{r})$ is the centrifugal acceleration, $2\vec{\omega}\times\vec{u}_R$ is the Coriolis acceleration, and the subscripts F and R denote the "fixed" and "rotating" reference frame from which quantities are measured, respectively.

The two non-inertial accelerations can be converted to:

$$\vec{\omega}\times(\vec{\omega}\times\vec{r}) = -\omega^2 z\langle\vec{k}\rangle - \omega^2 x\langle\vec{i}\rangle \tag{4}$$

$$2\vec{\omega}\times\vec{u} = -2\omega v\langle\vec{k}\rangle + 2\omega u\langle\vec{i}\rangle \tag{5}$$

The Navier–Stokes equations in a rotating frame of reference are then written as:

$$\hat{k}: u\frac{\partial u}{\partial z}+v\frac{\partial u}{\partial x}+w\frac{\partial u}{\partial y}-2\omega v-\omega^2 z=-\frac{1}{\rho}\frac{\partial P}{\partial z}+\nu\left(\frac{\partial^2 u}{\partial z^2}+\frac{\partial^2 u}{\partial x^2}+\frac{\partial^2 u}{\partial y^2}\right)$$
$$\hat{i}: u\frac{\partial v}{\partial z}+v\frac{\partial v}{\partial x}+w\frac{\partial v}{\partial y}+2\omega u-\omega^2 x=-\frac{1}{\rho}\frac{\partial P}{\partial x}+\nu\left(\frac{\partial^2 v}{\partial z^2}+\frac{\partial^2 v}{\partial x^2}+\frac{\partial^2 v}{\partial y^2}\right) \quad (6)$$
$$\hat{j}: u\frac{\partial w}{\partial z}+v\frac{\partial w}{\partial x}+w\frac{\partial w}{\partial y}=-\frac{1}{\rho}\frac{\partial P}{\partial y}+\nu\left(\frac{\partial^2 w}{\partial z^2}+\frac{\partial^2 w}{\partial x^2}+\frac{\partial^2 w}{\partial y^2}\right)$$

2.2.2. Scaling analysis

In dimensionless forms of the governing equations, one can identify a group of dimensionless parameters that play an important role in determining a flow field and thus obtain a reduced form of the equations by casting relatively unimportant terms. This can be achieved by non-dimensionalizing the equations.

The characteristic quantities are listed as:

- Characteristic dimensions: L_0 (radial distance of channel outlet), W_0 (channel width), and D_0 (channel depth). Note that L_0 is much greater than W_0 or D_0 (i.e., $L_0 \gg W_0, D_0$).
- Characteristic velocities: U_c (velocity in z-direction, i.e., downchannel velocity), V_c (velocity in x-direction), and W_c (velocity in y-direction).
- Characteristic pressure: $P_c = \rho\omega^2 L_0^2$.

The dimensionless variables are defined as:

$$z^*=\frac{z}{L_0},\quad x^*=\frac{x}{W_0},\quad y^*=\frac{y}{D_0} \quad (7)$$
$$u^*=\frac{u}{U_c},\quad v^*=\frac{v}{V_c},\quad w^*=\frac{w}{W_c}$$

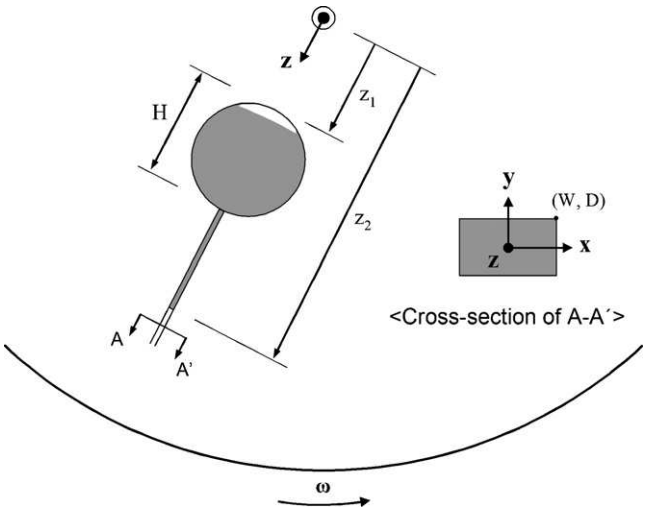

Fig. 2. Schematic diagram of a liquid being pumped through a rectangular channel embedded in a disk spinning at an angular frequency of ω. The dimensional parameters associated with finding the maximum velocity of the moving liquid are as follows: z_1 and z_2 are the inner and outer radii of the liquid extent, respectively; the rectangular channel has the width of $2W$ and the height of $2D$, and H is the "head" of liquid in the reservoir. Note that the head loss due to the liquid fed up to the junction is ignored for convenient analysis.

The dimensionless continuity equation is written as:

$$\frac{U_c}{L_0}\frac{\partial u^*}{\partial z^*}+\frac{V_c}{W_0}\frac{\partial v^*}{\partial x^*}+\frac{W_c}{D_0}\frac{\partial w^*}{\partial y^*}=0 \quad (8)$$

Conservation of mass requires that all coefficients in Eq. (8) be of the same order of magnitude.

$$\frac{U_c}{L_0}\sim\frac{V_c}{W_0}\sim\frac{W_c}{D_0} \quad (9)$$

The dimensionless form of Navier–Stokes equations in the rotating reference frame can be written as:

$$\left(\frac{U_c}{\omega L_0}\right)^2\{Conv.^*\}-2\left(\frac{U_c}{\omega L_0}\right)\left(\frac{W_0}{L_0}\right)v^*-z^* = -\frac{\partial P^*}{\partial z^*}+\left(\frac{U_c}{\omega L_0}\right)^2\left(\frac{L_0}{D_0}\right)\left(\frac{1}{Re}\right)\times\left\{\left(\frac{D_0}{W_0}\right)^2\frac{\partial^2 u^*}{\partial x^{*2}}+\frac{\partial^2 u^*}{\partial y^{*2}}\right\} \quad (10)$$

$$\left(\frac{U_c}{\omega L_0}\right)^2\left(\frac{W_0}{L_0}\right)^2\{Conv.^*\}+2\left(\frac{U_c}{\omega L_0}\right)\left(\frac{W_0}{L_0}\right)u^*-\left(\frac{W_0}{L_0}\right)^2 x^* = -\frac{\partial P^*}{\partial x^*}+\left(\frac{U_c}{\omega L_0}\right)\left(\frac{\nu}{\omega {L_0}^2}\right)\left\{\frac{\partial^2 v^*}{\partial x^{*2}}+\left(\frac{W_0}{D_0}\right)^2\frac{\partial^2 v^*}{\partial y^{*2}}\right\} \quad (11)$$

$$\left(\frac{U_c}{\omega L_0}\right)^2\left(\frac{D_0}{L_0}\right)^2\{Conv.^*\} = -\frac{\partial P^*}{\partial y^*}+\left(\frac{U_c}{\omega L_0}\right)\left(\frac{D_0}{L_0}\right)\left(\frac{\nu}{\omega {L_0}^2}\right)\times\left\{\left(\frac{D_0}{W_0}\right)^2\frac{\partial^2 w^*}{\partial x^{*2}}+\frac{\partial^2 w^*}{\partial y^{*2}}\right\} \quad (12)$$

where $U_c/\omega L_0$ is the ratio of downchannel velocity to circumferential velocity of liquid at channel outlet, $Conv.^*$ is the non-dimensionalized convection term of the Navier–Stokes equations, and Re is the Reynolds number ($=U_c D_0/\nu$). In Table 1, we compare the coefficients in Eq. (10) and point out that the convective and Coriolis acceleration terms are approximately 1 or 2 orders of magnitude smaller than that of the viscous term which is approximately of order 10^{-1}. All coefficients in Eqs. (11) and (12) also are at least 3 orders of magnitude smaller than those of the pressure gradients. Therefore, the dimensionless

Table 1
Comparison of coefficients in Eq. (10) with respect to angular frequencies

Angular frequency, ω (rad s^{-1})	Convective term: $\left(\frac{U_c^*}{\omega L_0}\right)^2$	Coriolis term: $2\left(\frac{U_c}{\omega L_0}\right)\left(\frac{W_0}{L_0}\right)$	Viscous term: $\left(\frac{U_c}{\omega L_0}\right)^2\left(\frac{L_0}{D_0}\right)\left(\frac{1}{Re}\right)$
40	3.00E−03	1.11E−03	0.11
50	4.68E−03	1.38E−03	0.11
60	6.74E−03	1.66E−03	0.11
70	9.18E−03	1.94E−03	0.11
80	1.20E−02	2.22E−03	0.11
90	1.52E−02	2.49E−03	0.11
100	1.87E−02	2.77E−03	0.11
110	2.27E−02	3.05E−03	0.11
120	2.70E−02	3.32E−03	0.11

* U_c is a mean velocity and is calculated based on Eq. (19).

Navier–Stokes equation can be reduced to:

$$-z^*=-\frac{\partial P^*}{\partial z^*}+\left(\frac{U_c}{\omega L_0}\right)^2\left(\frac{L_0}{D_0}\right)\left(\frac{1}{Re}\right)\left\{\frac{\partial^2 u^*}{\partial x^{*2}}+\frac{\partial^2 u^*}{\partial y^{*2}}\right\}$$
$$\frac{\partial P^*}{\partial x^*}=0 \qquad (13)$$
$$\frac{\partial P^*}{\partial y^*}=0$$

As seen in Eq. (13), the relative contribution of the convective and Coriolis forces is so small in the range of our test frequencies (i.e., 40–120 rad s^{-1}) that those terms can be ignored during the scaling analysis. However, Eq. (13) is only valid for moderately low angular frequencies of the disk because the size of the convective and Coriolis terms will rapidly grow similar to that of the viscous term (i.e., order of 10^{-1}) at elevated angular frequencies. Note that U_c and Re depend on ω.

2.2.3. Computation of liquid velocity

In computing the velocity of the liquid flowing though a rectangular microchannel on a rotating disk as seen in Fig. 2, the followings are assumed that the channel entrance effect is negligible and that the disk is accelerated rapidly enough to a constant angular velocity so that transient effects can be ignored. The Navier–Stokes equation in the non-inertial system is then reduced to:

$$-\rho\omega^2 z=-\frac{dP}{dz}+\mu\left(\frac{\partial^2 u}{\partial x^2}+\frac{\partial^2 u}{\partial y^2}\right) \qquad (14)$$

where z is the radial distance from the center of rotation, ρ the density, and μ is the viscosity of the liquid. Eq. (13) indicates that the velocity (u) is independent of z (i.e., $u=u(x, y)$). Integration of Eq. (14) over z from z_1 to z_2 gives:

$$\frac{\partial^2 u}{\partial x^2}+\frac{\partial^2 u}{\partial y^2}=\frac{1}{\mu}\frac{\Delta P}{\Delta z}-\frac{\omega^2}{\nu}\bar{z}=C_0 \qquad (15)$$

where Δz is the radial extent of the liquid ($\Delta z=z_2-z_1$), $\bar{z}$ is the average distance of the liquid extent from the center of rotation ($\bar{z}=(z_1+z_2)/2$), and C_0 is a constant. To get a solution, we let:

$$u(x, y)=u_h(x, y)+u_p(x) \qquad (16)$$

thereby decomposing Eq. (15) into two separate equations:

$$\frac{\partial^2 u_h}{\partial x^2}+\frac{\partial^2 u_h}{\partial y^2}=0$$
$$\frac{\partial^2 u_p}{\partial x^2}=C_0 \qquad (17)$$

By applying the following no-slip and symmetry boundary conditions:

$$u(x, D)=0$$
$$u(W, y)=0$$
$$\frac{\partial u}{\partial x}(0, y)=0 \qquad (18)$$
$$\frac{\partial u}{\partial y}(x, 0)=0$$

The velocity distribution of the liquid flowing through the microchannel is then obtained as:

$$u(x, y)=\frac{C_0}{2}(x^2-W^2)+\frac{2C_0}{W}\sum_{n=0}^{\infty}\frac{(-1)^n}{\lambda_n^3\cdot\cosh(\lambda_n D)}\cdot\cos(\lambda_n x)\cdot\cosh(\lambda_n y), \qquad (19)$$

$$\lambda_n=\left(n+\frac{1}{2}\right)\frac{\pi}{W}$$

Here, we further assume there is no net pressure drop across the liquid extent (i.e., $P_1=P_2=P_a$ where P_a is ambient pressure) although a local pressure gradient does exit. The maximum velocity occurs at the center of the channel cross-section:

$$u_{max}=u(0, 0)=\frac{W^2\bar{z}}{2\nu}\omega^2\underbrace{\left(1-\frac{4}{\pi^3}\sum_{n=0}^{\infty}\frac{(-1)^n}{(n+1/2)^3\cdot\cosh((n+1/2)\pi D/W)}\right)}_{F(D/W)} \qquad (20)$$

where $F(D/W)$ represents a geometrical factor depending on the aspect ratio D/W of the channel cross-section. We now compute the Coriolis force ($\vec{f}_{\mathrm{cor}} = -2\rho\vec{\omega} \times \vec{u}$) of the liquid reaching the junction using the maximum velocity in Eq. (20), and centrifugal force ($\vec{f}_{\mathrm{cen}} = -\rho\omega^2\vec{r}$) based on its radial distance from the center. The ratio of the Coriolis to the centrifugal force is found as a linear function of angular frequency of the disk:

$$\frac{\left|\vec{f}_{\mathrm{cor}}\right|}{\left|\vec{f}_{\mathrm{cen}}\right|} = F\left(\frac{D}{W}\right) \cdot \frac{W^2\bar{z}}{\nu \cdot z_2} \cdot \omega \tag{21}$$

In Fig. 3, Coriolis-to-centrifugal force ratios calculated using channel dimensions ($D = 80\,\mu\mathrm{m}$, $W = 215\,\mu\mathrm{m}$, $z_1 = 29\,\mathrm{mm}$, $z_2 = 42.5\,\mathrm{mm}$) and kinematic viscosity of water ($1.0 \times 10^{-6}\,\mathrm{m^2\,s^{-1}}$) are listed in parenthesis below the corresponding angular frequencies. Fig. 3 also shows that the flow switching valve starts performing at an angular frequency of $80\,\mathrm{rad\,s^{-1}}$. At this frequency, the entire flow past the junction bends to an intended outlet chamber with about 50% success rate. This is a significantly reduced frequency compared to the threshold frequency (i.e., $350\,\mathrm{rad\,s^{-1}}$) measured in the previous work [19], which is made possible due to our unique junction geometry.

Above $90\,\mathrm{rad\,s^{-1}}$ (the force ratio of 0.47), the switching valve allows the liquid in a common reservoir to flow only to an outlet chamber located to the left of the junction for a disk spinning in a counter-clockwise direction. The flow would be to an outlet chamber located to the right of the junction for a disk spinning in the clockwise direction as shown in Fig. 4.

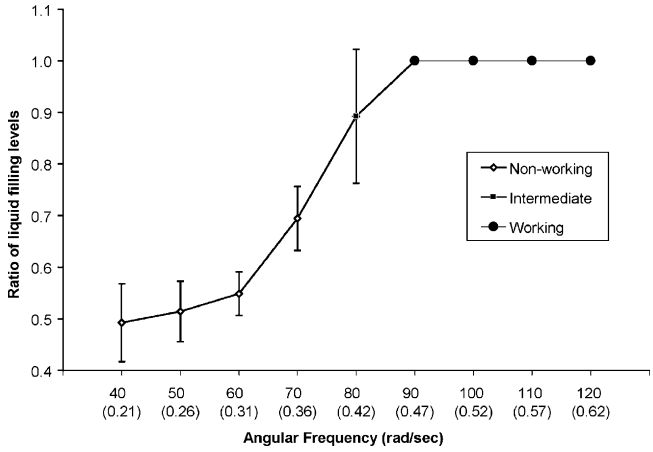

Fig. 3. Ratio of the liquid level filling a selected reservoir to the sum of filling levels in both reservoirs versus angular frequency. The ratio is chosen as $h_{\mathrm{L}}/(h_{\mathrm{L}} + h_{\mathrm{R}})$ for counter-clock wise rotation of a disk, where h_{L} and h_{R} are the liquid levels measured in the reservoir located to the left/right of the junction, respectively. The Coriolis-to-centrifugal force ratio for corresponding frequency is shown in parenthesis. Three different shapes of marks (i.e., ◊, ■, ●) indicate "non-working", "intermediate", and "working" states, respectively. At the non-working state, a liquid hits the tip of separation wall and splits into two streams due to insufficient Coriolis force impact. The intermediate status is a transition point where Coriolis force becomes influential to make a liquid flow bend but is not large enough for complete flow switching. Thus, both non-working and working statuses co-exist in this regime. Entering the working state, liquid flows are directed into an intended outlet chamber without showing any liquid split, which is referred to as 100% liquid switching in the context. The angular distance between liquid flow and separation wall increases with increased angular frequencies.

2.3. Flow valving: fluidic capacitance

Often, working with hydrophobic surfaces in microflow is not very convenient, especially when the objective is the mixing of two liquids. The reason is that an air pocket [22] may be created around the junction where the two liquids meet, thereby preventing the mixing unless they reach the junction simultaneously. We can, however, take advantage of the air pocket trapped in the channel as another means for switching the direction of flow. Fluidic capacitance mediated by an air plug can be generated between two liquids sequentially fed into a common channel. This capacitance is maintained through a channel-chamber coupling that allows the centripetal pressure exerted on the first liquid to hold up the capacitance.

As shown in Fig. 5, the junction has a non-symmetric configuration: a main channel (wide and straight) and a branch channel (narrow and tilted). Due to the larger capillary barrier developed at the entrance of the branch channel, a disk spinning at

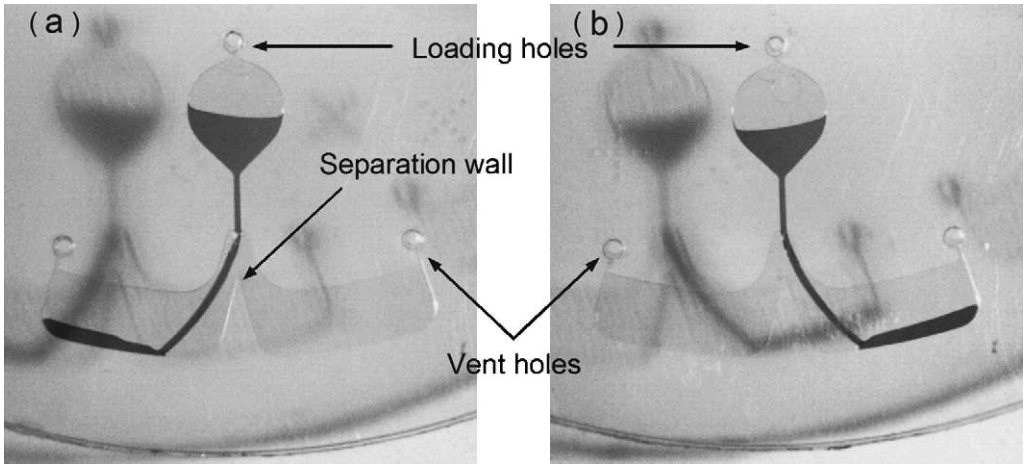

Fig. 4. Still images of disks performing flow switching: (a) disk spinning in counter-clockwise direction at $180\,\mathrm{rad\,s^{-1}}$; (b) disk spinning in clockwise direction at $200\,\mathrm{rad\,s^{-1}}$.

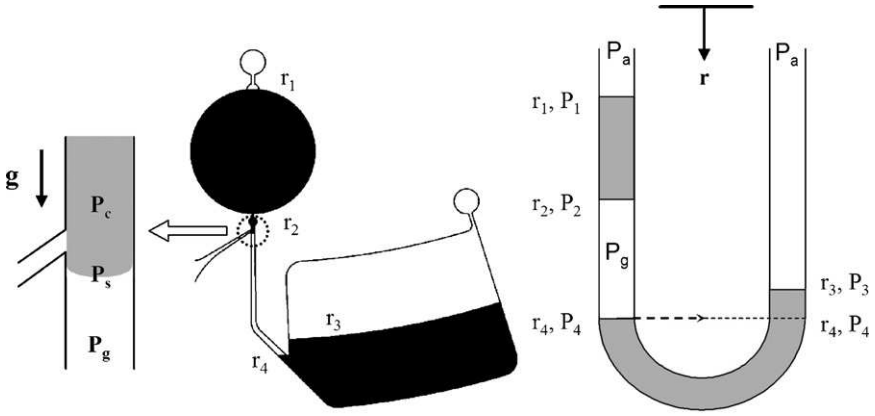

Fig. 5. Illustrative view of the second liquid being pumped into a non-symmetric junction on a rotating disk, following the first liquid filling the first (right) chamber. The monometer model on the right depicts a static pressure balance for the liquid–air–liquid arrangement under centrifugation. P_c is the centrifugal pressure, P_s is the capillary pressure, P_g is the gas pressure, and P_a is the atmospheric pressure.

52 rad s^{-1} drives the first liquid only through the main channel without crosstalk with the branch channel shown in Fig. 6(a). A small amount of excess liquid occupies a short portion (i.e., the same level as r_3 in Fig. 5) of the main channel coupled to the first chamber at this stage. Afterwards, during the introduction of the second liquid, the excess amount of the first liquid is pushed down to a lower level (i.e., r_4 below r_3 as shown in Fig. 5).

In the conventional analysis of centrifuge-based fluid propulsion [16], the balance of centrifugal pressure (P_c) induced by a spinning disk and the capillary pressure (P_s) that arises at the junction due to interfacial tension has been considered. However, the gas pressure (P_g) has not played a part in the pressure balance due to the existence of air vent holes connected to the participating chambers. In our case, when the second fluid is pumped in, the gas pressure at the radial distance r_2 (see Fig. 5) is expressed as:

$$P_g = P_2 = \rho\omega^2 \cdot \Delta r_{12} \cdot \bar{r}_{12} + P_a - P_s \tag{22}$$

with $\Delta r_{12} = r_2 - r_1$, $\bar{r}_{12} = (r_1 + r_2)/2$, and $P_s = 4\gamma \cos\theta / D_H$ where γ is the surface tension, θ the liquid contact angle, and D_H the hydraulic diameter ($D_H = 4A/P$, A is the cross-sectional area and P is the perimeter of the rectangular channel). P_g is the pressure in the air pocket trapped in the channel and is assumed to be uniform. P_a is the atmospheric pressure. From the monometer model describing the liquid–air–liquid arrangement in Fig. 5, the P_g at the radial distance r_4 is given by

$$P_g = P_4 = \rho\omega^2 \cdot \Delta r_{34} \cdot \bar{r}_{34} + P_a - P_s \tag{23}$$

with $\Delta r_{34} = r_4 - r_3$ and $\bar{r}_{34} = (r_3 + r_4)/2$. Note that there is no net effect of the negative capillary pressures on the gas pressure as the dimensions (cross-section) are constant along the main channel.

Equating Eqs. (22) and (23) gives a critical condition for preventing the second liquid from flowing through the main channel that is obtained as:

$$\Delta r_{12} \cdot \bar{r}_{12} = \Delta r_{34} \cdot \bar{r}_{34} \tag{24}$$

As mentioned earlier, the level of the excess liquid in the main channel moves down until Eq. (24) is satisfied. Upon satisfying this condition, the second fluid will not proceed further into the main channel and thus will be redirected to an alternate path, the branch channel—resulting in flow switching. The air pocket becomes compressed during this process but its compression rate is negligible at the operational frequencies required for the flow switching. Fig. 6(b) shows the instant of flow switching of the second liquid by the fluidic capacitance of a trapped air plug.

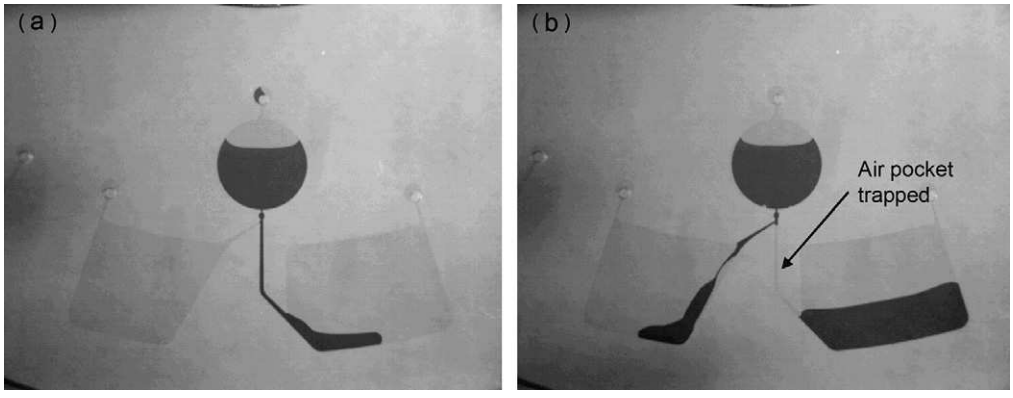

Fig. 6. Fluidic capacitance method for flow switching (a) the first liquid is pumped through the main channel without interacting with the branch channel (b) the second liquid flows into the branch channel due to the fluidic capacitance of a trapped air pocket.

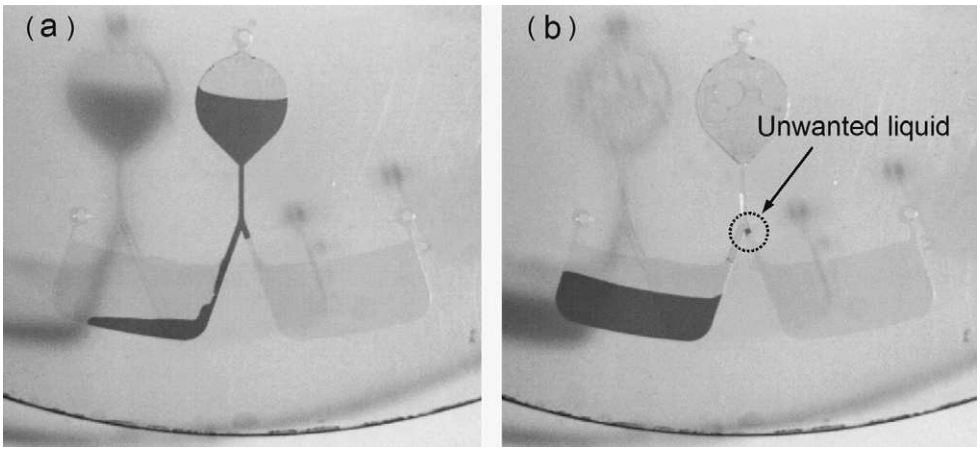

Fig. 7. Flow switching in a planar junction of symmetry for a disk spinning in counter-clockwise direction at 310 rad s^{-1}. Dimensions of channel, chamber, and their radial locations are identical to those of the double-layered disk.

3. Results and discussion

We investigated two different schemes of valves for switching of liquid flow in a centrifugal platform that enable a fluid being pumped to flow solely into a selected path in a junction where a common inlet and two outlet channels meet. The key feature of Coriolis force-induced method lies in the double-layered junction structure that consists of a common inlet channel (i.e., narrow and thin) and two symmetric outlet chambers (i.e., wide and thick). Such an arrangement plays an important role in performing the flow valving with the following advantages: (1) a flow past the junction arises only at the surface of sealing material, thereby making the flow more easily bend to a desired chamber due to reduced contact area of the fluid, (2) Coriolis force can also be maximized with the significantly increased flow rate at a given angular frequency of the disk, and (3) any introduction of liquid into an unintended channel that often occurs in a planar junction structure (see Fig. 7) can be prevented. This is an essential requirement for the flow-switching valve to be used in bioassays where specific target materials need to be separated since any unwanted liquid remaining serves as a source of potentially serious contamination. As shown in Fig. 8, the comparison of two disks with different junction structures (say, 2D versus 3D) for flow switching performance shows that unbalanced liquid splits were observed in the planar junction disk that rotated even at a highly elevated frequency of 310 rad s^{-1}. This result is in disagreement with the previous work [19], which can be attributed to difference in channel geometries and surface energy of the substrates. But, it appears to be extremely difficult to divert all the liquid into only a designated outlet of the planar junction on a PDMS substrate. On the other hand, in a double-layered junction, an entire flow can be switched simply by changing a rotational direction of a disk which spins above the threshold frequency.

But, a disk spinning just above the threshold frequency inherently exhibits a residual liquid plug at the end of inlet channel due to a capillary pressure developed at the junction. In order to remove the residual liquid problem, the disk is required to spin at higher frequencies and our empirical observation showed that no liquid plug remained beyond a frequency of 180 rad s^{-1}.

The fluidic capacitance method depends little on the angular frequency but requires careful geometrical consideration to determine a flow path in a planar junction structure. Its performance entirely relies on the following conditions: (1) non-symmetric channel geometry (i.e., different width and tilting angle), (2) sequence of liquid pumped to its designated chamber, and (3) pressure balance in liquid–air–liquid arrangement. Also, the volume of the first liquid should be carefully controlled in conjunction with the first chamber (e.g., shape and radial position) such that an excess liquid can occupy a short portion of the main channel coupled to the first chamber when the first liquid is completely pumped down. This is to set up liquid–air–liquid arrangement during the introduction of the second liquid. As soon as the arrangement is formed, the excess liquid is pushed down until a critical condition (i.e., Eq. (24)) is met, which results in switching of the second liquid into a branch channel.

This method inherently leaves a tiny liquid plug in the main channel (i.e., a part of the second liquid extending from the branch channel entrance to the top of air pocket, see Fig. 6 (b))

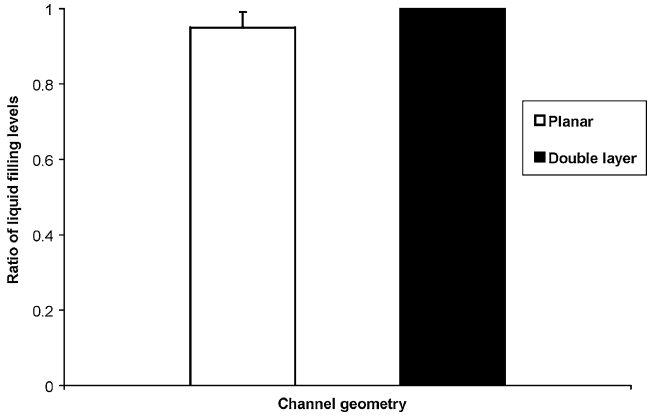

Fig. 8. Comparison of planar (2D) and double-layered (3D) junction structures for the ratio, $h_L/(h_L + h_R)$. Both disks spin in a counter-clockwise direction at 310 rad s^{-1}.

at the end of the switching event. Its volume roughly amounts to 6% of the second liquid's volume. Note that this remaining liquid would not be regarded as a source of contamination for subsequent applications but represent a slight loss of anticipated material (e.g., eluted DNA in solid phase DNA extraction). Our experimental observation shows that flow-switching tests ($n = 4$) were all successful.

4. Conclusion

A valve for switching the flow of a liquid was demonstrated on a centrifugal microfluidic platform. Two different approaches were introduced: Coriolis force and fluidic capacitance. The Coriolis force-based method relies on the frequency and direction of a rotating disk with a double-layered symmetric junction while the fluidic capacitance method takes advantage of the centripetal pressure acting on the first fluid filling the main channel and the connecting chamber in a non-symmetric junction arrangement.

We anticipate that the combined use of these flow switching valves and affinity-based separation techniques (e.g., adsorption of DNA on a silica matrix, followed by elution) will have great potential in rapid bioassays and biomedical diagnostic applications that require the extraction of specific target biomoleclues.

Acknowledgement

We thank our colleagues in BioMEMS group at University of California, Irvine, especially Kuosheng Ma and Guangyao Jia, for experimental assistance.

References

[1] D.J. Harrison, A. Van Den Berg, microTAS '98, Banff (Canada), 1998.
[2] J.V. Zoval, M.J. Madou, Centrifuge-based fluidic platforms, Proc. IEEE 92 (2004) 140–153.
[3] A. Manz, C.S. Effenhauser, N. Burggraf, D.J. Harrison, K. Seiler, K. Fluri, Electroosmotic pumping and electrophoretic separations for miniaturized chemical-analysis systems, J. Micromech. Microeng. 4 (1994) 257–265.
[4] M.G. Pollack, R.B. Fair, A.D. Shenderov, Electrowetting-based actuation of liquid droplets for microfluidic applications, Appl. Phys. Lett. 77 (2000) 1725–1726.
[5] D.J. Harrison, K. Fluri, K. Seiler, Z.H. Fan, C.S. Effenhauser, A. Manz, Micromachining a miniaturized capillary electrophoresis-based chemical-analysis system on a chip, Science 261 (1993) 895–897.
[6] X.B. Wang, J. Yang, Y. Huang, J. Vykoukal, F.F. Becker, P.R.C. Gascoyne, Cell separation by dielectrophoretic field-flow-fractionation, Anal. Chem. 72 (2000) 832–839.
[7] N.T. Nguyen, X.Y. Huang, T.K. Chuan, MEMS-micropumps: a review, J. Fluids Eng.-Trans. ASME 124 (2002) 384–392.
[8] N.T. Nguyen, T.Q. Truong, A fully polymeric micropump with piezoelectric actuator, Sens. Actuators B-Chem. 97 (2004) 139–145.
[9] W.I. Jang, C.A. Choi, C.H. Jun, Y.T. Kim, M. Esashi, Surface micromachined thermally driven micropump, Sens. Actuators A-Phys. 115 (2004) 151–158.
[10] D.C. Roberts, H.Q. Li, J.L. Steyn, O. Yaglioglu, S.M. Spearing, M.A. Schmidt, N.W. Hagood, A piezoelectric microvalve for compact high-frequency, high-differential pressure hydraulic micropumping systems, J. Microelectromech. Syst. 12 (2003) 81–92.
[11] E.T. Carlen, C.H. Mastrangelo, Surface micromachined paraffin-actuated microvalve, J. Microelectromech. Syst. 11 (2002) 408–420.
[12] C. Goll, W. Bacher, B. Bustgens, D. Maas, R. Ruprecht, W.K. Schomburg, An electrostatically actuated polymer microvalve equipped with a movable membrane electrode, J. Micromech. Microeng. 7 (1997) 224–226.
[13] Y.Y. Feng, Z.Y. Zhou, X.Y. Ye, H.J. Xiong, Passive valves based on hydrophobic microfluidics, Sens. Actuators A-Phys. 108 (2003) 138–143.
[14] T. Vestad, D.W.M. Marr, J. Oakey, Flow control for capillary-pumped microfluidic systems, J. Micromech. Microeng. 14 (2004) 1503–1506.
[15] D.C. Duffy, H.L. Gillis, J. Lin, N.F. Sheppard, G.J. Kellogg, Microfabricated centrifugal microfluidic systems: characterization and multiple enzymatic assays, Anal. Chem. 71 (1999) 4669–4678.
[16] M.J. Madou, L.J. Lee, S. Daunert, S. Lai, C.H. Shih, Design and fabrication of CD-like microfluidic platforms for diagnostics: microfluidic functions, Biomed. Microdevices 3 (2001) 245–254.
[17] D.C. Duffy, J.C. McDonald, O.J.A. Schueller, G.M. Whitesides, Rapid prototyping of microfluidic systems in poly(dimethylsiloxane), Anal. Chem. 70 (1998) 4974–4984.
[18] T. Rosqvist, S. Johansson, Soft micromolding and lamination of piezoceramic thick films, Sens. Actuators A-Phys. 97–98 (2002) 512–519.
[19] T. Brenner, T. Glatzel, R. Zengerle, J. Ducree, Frequency-dependent transversal flow control in centrifugal microfluidics, Lab on a Chip 5 (2005) 146–150.
[20] J. Ducree, T. Brenner, S. Haeberle, T. Glatzel, R. Zengerle, Multilamination of flows in planar networks of rotating microchannels, Microfluid. Nanofluid. 2 (2006) 78–84.
[21] J. Ducree, S. Haeberle, T. Brenner, T. Glatzel, R. Zengerle, Patterning of flow and mixing in rotating radial microchannels, Microfluid. Nanofluid. 2 (2006) 97–105.
[22] J. Melin, N. Roxhed, G. Gimenez, P. Griss, W. van der Wijngaart, G. Stemme, A liquid-triggered liquid microvalve for on-chip flow control, Sens. Actuators B-Chem. 100 (2004) 463–468.

Biographies

Dr. Jitae Kim received his BS degree from mechanical engineering department, Hanyang University in South Korea (1998) and his MS degree from aerospace and mechanical engineering department, University of Southern California (2001). He obtained his PhD in mechanical and aerospace engineering from the University of California, Irvine (2006). His research interests include microfluidics, lab-on-a-chip applications, and relevant microfabrication technologies.

Dr. Horacio Kidon received his PhD degree in agricultural and environmental chemistry from the University of California, Davis in 1999. His BS and MS degrees, both in biological sciences, are from Stanford University (1987, 1988). He currently conducts research on a part-time basis in the area of centrifugal fluidic systems at the University of California, Irvine where his academic appointment is that of a research specialist. Horacio has work experience in the environmental regulatory field and currently serves as CEO of RotaPrep, Inc. in Tustin, California; a company that develops and sells sample preparation products for the life sciences markets.

Dr. Roger H. Rangel is a professor in the departments of mechanical & aerospace engineering and of chemical engineering & material science at the University of California, Irvine. He received a PhD and MS in mechanical engineering from the University of California at Berkeley (1985, 1983), and a degree in mechanical engineering from Simon Bolivar University in Venezuela (1981). His interests and research include droplet and spray vaporization and combustion, liquid-metal droplet solidification in materials processing, aerosol condensation, liquid atomization, and other dispersed multiphase flows.

Dr. Marc J. Madou before joining UCI as the chancellor's professor in mechanical and aerospace engineering, Dr. Madou was vice president of advanced technology at Nanogen in San Diego, California. He specializes in the application of miniaturization technology to chemical and biological problems (BIO-MEMS). He is the author of several books in this burgeoning field he helped pioneer both in academia and in industry. He founded several micromachining companies and has been on the board of many more. Many of his colleagues became well known in their own right in academia and through successful MEMS start-ups. Madou was the founder of the SRI International's microsensor department, founder and president of Teknekron Sensor Development Corporation (TSDC), visiting miller professor at UC Berkeley and endowed chair at the Ohio State University (professor in chemistry and materials science and engineering). He has just started the third edition of "Fundamentals of Microfabrication," an introduction to MEMS which has become known as the "bible" of micromachining. Some of Dr. Madou's recent research work involves artificial muscle for responsive drug delivery, a compact disc-based fluidic platform and a solid state pH electrode based on IrO_x. To find out more about those recent research projects, visit **www.biomems.net**. At UCI, Dr. Madou works on carbon-MEMS, a CD based fluidic platform, solid state pH electrodes, artificial muscle for responsive drug delivery and integrating fluidics with DNA arrays as well as researching label–free assays for the molecular diagnostics platform of the future.